A Novel CDK2/9 Inhibitor CYC065 Causes Anaphase Catastrophe and Represses Proliferation, Tumorigenesis, and Metastasis in Aneuploid Cancers A C

Masanori Kawakami[1,2], Lisa Maria Mustachio[1], Yulong Chen[1], Zibo Chen[1,2], Xiuxia Liu[2], Cheng-Hsin Wei[2], Jason Roszik[3,4], Adam S. Kittai[5], Alexey V. Danilov[5], Xiaoshan Zhang[6], Bingliang Fang[6], Jing Wang[7], John V. Heymach[1], Liliya Tyutyunyk-Massey[2], Sarah J. Freemantle[8], Jonathan M. Kurie[1], Xi Liu[1,2], and Ethan Dmitrovsky[1,2,9]

ABSTRACT

Cyclin-dependent kinase 2 (CDK2) antagonism inhibits clustering of excessive centrosomes at mitosis, causing multipolar cell division and apoptotic death. This is called anaphase catastrophe. To establish induced anaphase catastrophe as a clinically tractable antineoplastic mechanism, induced anaphase catastrophe was explored in different aneuploid cancers after treatment with CYC065 (Cyclacel), a CDK2/9 inhibitor. Antineoplastic activity was studied in preclinical models. CYC065 treatment augmented anaphase catastrophe in diverse cancers including lymphoma, lung, colon, and pancreatic cancers, despite *KRAS* oncoprotein expression. Anaphase catastrophe was a broadly active antineoplastic mechanism. Reverse phase protein arrays (RPPAs) revealed that along with known CDK2/9 targets, focal adhesion kinase and Src phosphorylation that regulate metastasis were each repressed by CYC065 treatment. Intriguingly, CYC065 treatment decreased lung cancer metastases in *in vivo* murine models. CYC065 treatment also significantly reduced the rate of lung cancer growth in syngeneic murine and patient-derived xenograft (PDX) models independent of *KRAS* oncoprotein expression. Immunohistochemistry analysis of CYC065-treated lung cancer PDX models confirmed repression of proteins highlighted by RPPAs, implicating them as indicators of CYC065 antitumor response. Phospho-histone H3 staining detected anaphase catastrophe in CYC065-treated PDXs. Thus, induced anaphase catastrophe after CYC065 treatment can combat aneuploid cancers despite *KRAS* oncoprotein expression. These findings should guide future trials of this novel CDK2/9 inhibitor in the cancer clinic.

Introduction

Genomic instability is a hallmark of cancer (1). Genetically unstable cancer cells often have supernumerary centrosomes (2–6). At mitosis, these supernumerary centrosomes are clustered into two poles so that cancer cells preserve bipolar spindle assembly and undergo mitosis (7–11). We previously reported that cyclin-dependent kinase 1 or 2 (CDK1 or CDK2) antagonism inhibits centrosome clustering and forces aneuploid cancer cells with supernumerary centrosomes to undergo multipolar cell division and chromosome mis-segregation (12–16). This confers apoptotic death of daughter cells; this proapoptotic mechanism is called anaphase catastrophe (12, 13). Because anaphase catastrophe is augmented by preventing the clustering of preexisting supernumerary centrosomes, this mechanism preferentially affects aneuploid cancer cells while relatively sparing normal cells with two centrosomes (14).

CDK2 inhibitors such as seliciclib (12), dinaciclib (15), and CCT68127 (16) elicit antineoplastic effects against lung cancer cells through induced anaphase catastrophe. Effects by these agents were not prominently seen in immortalized pulmonary epithelial cells that had less chromosome instability than aneuploid lung cancer cells (12, 15, 16). Notably, *KRAS* oncoprotein-expressing lung cancer cells were sensitive to CDK2 inhibitors (12, 15, 16). This is because expression of the centrosome protein CP110, a direct phosphorylation target of CDK2 and a key mediator of anaphase catastrophe, is repressed in *KRAS*-mutant lung cancers as compared with KRAS wild-type (WT) tumors (14, 17, 18). Because treatment of *KRAS* mutant lung cancers is an unmet medical need (19, 20), this finding has translational implications.

Although pharmacologic inhibition of specific CDK family members such as CDK4/6 is FDA approved for a subset of breast cancers (21, 22), clinical validation of CDK2 inhibitors for cancer therapy is not yet established. First-generation pan-CDK and CDK2/7/9 inhibitors including dinaciclib and seliciclib, respectively, exerted dose-limiting toxicities in the clinic in part due to their relative lack of CDK2 specificity. To increase specificity for CDK2 inhibition, CCT68127, a next-generation CDK2/9 inhibitor was examined. Studies confirmed its antineoplastic efficacy without appreciable

[1]Department of Thoracic/Head and Neck Medical Oncology, The University of Texas MD Anderson Cancer Center, Houston, Texas. [2]Frederick National Laboratory for Cancer Research, Frederick, Maryland. [3]Department of Melanoma Medical Oncology, The University of Texas MD Anderson Cancer Center, Houston, Texas. [4]Department of Genomic Medicine, The University of Texas MD Anderson Cancer Center, Houston, Texas. [5]Knight Cancer Institute, Oregon Health and Science University, Portland, Oregon. [6]Department of Thoracic and Cardiovascular Surgery, The University of Texas MD Anderson Cancer Center, Houston, Texas. [7]Department of Bioinformatics and Computational Biology, The University of Texas MD Anderson Cancer Center, Houston, Texas. [8]University of Illinois, Urbana, Illinois. [9]Department of Cancer Biology, The University of Texas MD Anderson Cancer Center, Houston, Texas.

toxicities in a lung cancer mouse model (16). This is a preclinical tool compound that was not selected for clinical use (23).

Translational studies using clinically tractable CDK2 inhibitors were needed. CYC065 is such a next-generation reversible ATP competitive CDK2/9 inhibitor (Cyclacel; IC_{50} for CDK2: 5 nmol/L and CDK9: 26 nmol/L) available for clinical trial use; its structure appears in Supplementary Fig. S1A (24). CYC065 (Fadraciclib) is reported having a biochemical IC_{50} favoring inhibition of CDK2 ($IC_{50} = 4.5$ nm $\pm$ 0.4 nmol/L) over CDK9 ($IC_{50} = 26.2$ nmol/L $\pm$ 1.0 nmol/L). These potencies are 20-fold higher than the first-generation inhibitor Seliciclib (24). When used *in vivo* in treating cancer cells, the IC_{50} of CYC065 was 0.31 μmol/L versus an IC_{50} for Seliciclib of 13.3 μmol/L (24). The IC_{50} for lung cancer cell line growth-inhibitory effects were comparable with that reported in other tumor contexts (24). Seliciclib targeted in decreasing order CDK2, CDK7, and CDK9 (24). CYC065 did not appreciably affect CDK7, but preferentially inhibited CDK2 over CDK9 (24). Kinome profiling of 256 kinases (24) found that CYC065 was more selective for CDKs than for non-CDK enzymes.

CYC065 had preclinical antineoplastic activity against breast cancers (25–27) and uterine serous carcinomas (28). CYC065 activity is being examined in two phase I clinical trials; NCT02552953: a single agent trial in advanced cancers (not focused on lung cancer cases; ref. 29). NCT03739554 is a combined regimen with Venetoclax for relapsed/refractory chronic lymphocytic leukemia (30). CYC065 had clinical activity with acceptable toxicity (29).

This study advances prior work by exploring antineoplastic effects of the clinical-lead CDK2/9 inhibitor CYC065 in lung and other aneuploid cancer models. Anaphase catastrophe increased after CYC065 treatment of diverse aneuploid cancers. This was a broadly engaged antineoplastic mechanism observed despite *KRAS* oncoprotein expression. Interestingly, CYC065 treatment exhibited anti-metastatic activities. Multiple lung cancer patient-derived xenograft (PDX) models confirmed that CYC065 treatment triggers anaphase catastrophe and changes in expression of new and previously-known markers of CYC065 response. Thus, induced anaphase catastrophe induction is a promising strategy to combat human cancers like lung cancers that are aneuploid and often driven by the *KRAS* oncoprotein. Thus, CYC065 is a clinical-lead compound with promise to confer antineoplastic effects in the cancer clinic.

Materials and Methods

Cell culture

CYC065 was obtained from Cyclacel. Murine lung cancer cell lines ED1, LKR13, and KC2 cells were derived from lung cancers arising from WT cyclin E, Kras$^{LA1/+}$, and Kras$^{LA1/+}$; Cdkn1a$^{-/-}$ engineered mice, respectively, and were authenticated, as described previously (31–35). The 393P and 344SQ lung cancer cells were derived from a Kras$^{LA1/+}$; p53^{R172HΔG} engineered mouse (36). The ED1SQ4 cells were derived from ED1 cells (37). Human lung cancer cell lines (H522, H1299, Hop62, and A549), colon cancer cell lines (DLD1 and HCT116), pancreatic cancer cell lines (PSN1 and AsPC1), murine C10 pulmonary epithelial, and human BEAS-2B immortalized bronchial epithelial cells were purchased and authenticated by ATCC. Cells were cultured in RPMI1640 media with 10% fetal bovine serum (FBS) at 37°C with 5% CO_2 in a humidified incubator.

Proliferation assays

Logarithmically growing cells were seeded at optimized densities for each examined cell line onto individual wells of 12- or 96-well (for high-throughput test) tissue culture plates in triplicate. Cells were treated with CYC065 or vehicle (DMSO) 24 hours later. Proliferation was measured using the Cell Titer-Glo Luminescent Assay (Promega) after 48 to 72 hours of indicated drug exposures. Proliferation studies were independently replicated at least three times. For IC_{50} and IC_{70} values, multiple models were fitted on the basis of SE using the R software. For combination regimens with CYC065, indicated lung cancer cell lines were independently cultured with CYC065 or vehicle after Taxol (Paclitaxel) pretreatment at increasing concentrations and possible cooperative effects were examined (38).

Washout assays

Logarithmically growing cells were treated with CYC065 or vehicle for 24 hours and seeded at optimized densities onto individual wells of 24-well tissue culture plates after three washings with PBS. CYC065 or vehicle (DMSO) was independently added to the CYC065-treated or washout group. Proliferation was measured 48 hours later by Cell Titer-Glo Assay (Promega). Assays was performed in triplicate and in three independent experiments.

Apoptosis assays

Logarithmically growing cells were seeded at optimized densities for each examined cell line onto individual wells of 6-well tissue culture plates. Cells were treated with CYC065 or vehicle (DMSO) 24 hours later. Apoptosis assays were performed using the FITC Annexin V Apoptosis Detection Kit (BioLegend) after 48 hours of drug exposure. Independent triplicate replicates were done.

Cell-cycle analyses

Cells were fixed in ice-cold 70% ethanol and stained with propidium iodide/RNase Staining Solution (F10797; Thermo Fisher Scientific) with RNase A solution (Novagen) added at 100 μg/mL after fixation. DNA contents were measured using Gallios flow cytometer (Beckman Coulter) using FlowJo software (FlowJo, LLC) after 24 hours of drug exposure. G_1 phase synchronization was achieved in logarithmically growing A549 lung cancer cells treated with nocodazole 20 ng/mL (Sigma-Aldrich) for 4 hours with cells isolated by mitotic shake-off before seeding onto tissue culture plates for 2 hours before CYC065 or vehicle treatment. Independent triplicate replicate experiments were performed.

Multipolar anaphase assays

Cells were fixed, stained with anti–α-tubulin and γ-tubulin–specific antibodies along with Hoechst, and then mounted with Pro-Long Gold antifade reagent (P36934; Invitrogen). Stained cells were scored for multipolar anaphase cells using an Eclipse TE 2000-E microscope (Nikon). Primary antibodies were: α-tubulin (for single stain: T6199; Sigma-Aldrich; 1:1,000, for double staining with γ-tubulin: NB600–506; Novus Biologicals; 1:1,500) and γ-tubulin (T5326; Sigma-Aldrich; 1:1,000). Secondary antibodies were Texas red anti-murine IgG (H+L) (TI-2000; Vector Laboratories; 1:500), Alexa-Fluor 594 anti-rat IgG (A21209; Invitrogen; 1:1,000), and Fluorescein anti-murine IgG (FI-2000; Vector Laboratories; 1:100). Hoechst 33342 (62249; Thermo Fisher Scientific; 1:10,000) stained for DNA. Pro-Long Gold anti-fade reagent preserved immunofluorescence. Each assay was done in triplicate. Independent triplicate replicate experiments were performed.

Senescence assays

Senescence was measured using a β-Galactosidase Staining Kit (Cell Signaling Technologies). For quantification of senescence, cells were

exposed to 100 nmol/L Bafilomycin (No. B1793; Sigma-Aldrich) for 45 minutes, stained with 100 nmol/L C12FDG (Thermo Fisher Scientific) for 2 hours and analyzed by flow cytometry. Assays were in triplicate with independent triplicate replicates.

Ki-67 assay

Logarithmically growing cells were seeded on cover slips 24 hours before vehicle or CYC065 treatments. Cells were fixed in ice-cold methanol and stained with anti–Ki-67 antibody (No. ab15580; Abcam). Stained cells were scored using an Axio Observer 7 confocal microscope (Zeiss). Trypan blue staining was also done. Assays were performed in triplicate with three independent replicates.

Expression plasmids and transfection

Expression plasmids for CDK2 and CDK9 and the empty vector were purchased from GeneCopoeia (CDK2: EX-A0035-M95, CDK9: EX-M0107-M95, empty vector: EX-NEG-M95). Transient transfection was achieved using jet PRIME (Polyplus transfection).

Immunoblot analyses

Lysates were in RIPA buffer with Halt Protease and Phosphatase Inhibitor Cocktail (Thermo Fisher Scientific). These were size-fractionated by SDS-PAGE and transferred to nitrocellulose membranes. Membranes were probed with indicated antibodies and visualized using Clarity Western ECL Substrate (Bio-Rad). Primary antibodies were: CDK2 (No. 2546; Cell Signaling Technology; 1:1,000), CDK9 (No. 2316; Cell Signaling Technology; 1:1,000), and β-actin (No. 3700; Cell Signaling Technology; 1:1,000). Secondary antibodies were goat anti-rabbit IgG (170-6515; Bio-Rad; 1:2,000) and goat anti-mouse IgG (170-6516; Bio-Rad; 1:5,000).

Reverse phase protein arrays

Lysates were arrayed on nitrocellulose-coated slides and probed with 305 unique antibodies with analysis done as before (39–41).

Scratch assays

Confluent monolayers of cells were scratched using a sterile 200-μL pipette tip to produce a wounded area of constant length. Cells were photographed 6 to 12 hours later. Wounded area filling was measured using Adobe Photoshop software. Experiments were in triplicate and with three independent replicates.

Migration and invasion assays

Cells (1×10^5) were cultured without FBS in the upper wells of Transwell and Matrigel chambers (Corning) and allowed to migrate and invade with 10% FBS supplemented lower wells. After 18 hours of incubation, migrating, or invading, cells were stained with 0.5% crystal violet. Migration and invasion were quantified by the absorbance of crystal violet stain. Studies were in triplicate with three independent replicates.

Lung cancer murine syngeneic and PDX models

KRAS mutant murine lung cancer 393P cells and KRAS WT murine lung cancer ED1SQ4 cells were individually infected with luciferase lentivirus (Cellomics Technology) and selected with puromycin. The 393P (1×10^6) and ED1SQ4 (1×10^6) stable transfectants were each injected subcutaneously into 6- to 8-week-old male immunocompetent 129S2/SVPasCrl mice (Charles River Laboratories) and female immunocompetent FVB/N mice (Jackson Laboratory), respectively. Lung cancer PDXs were established from lung cancer clinical specimens that were surgically resected at the University of Texas MD

Anderson Cancer Center (42, 43). Tumors were cut and implanted into the flank subcutaneous space of athymic nude or NSG mice (Jackson Laboratory); mice were monitored for tumor growth. Correlative scientific studies were approved by the MD Anderson Cancer Center Institutional Review Board. All experiments were conducted following an Institutional Animal Care and Use Committee (IACUC)-approved protocol.

In vivo tumor growth assays

Mice with palpable tumors were treated with CYC065 (55 mg/kg for 129S2/SVPasCrl mice; 75 mg/kg for FVB/N, athymic nude, and NSG mice) or vehicle (water) daily for 3 to 4 weeks by oral gavage ($n = 10$ per group). Body weights and tumor volumes were measured with tumor volume (V) calculated as $V = (\text{length} \times \text{width}^2)/2$. Bioluminescence imaging was by D-Luciferin (Gold Biotechnology) and IVIS Lumina (Xenogen) and Living Imaging software (Xenogen) under 2% isoflurane. Tumors were excised and weighed from sacrificed mice. Independent replicate experiments were performed following an IACUC-approved protocol.

Metastasis assays

Metastasis-prone murine lung cancer 344SQ cells (4×10^3) were tail–vein injected into 6- to 8-week-old male immunocompetent 129S2/SVPasCrl mice (Charles River Laboratories). Mice were treated with CYC065 (55 mg/kg) or vehicle (water) daily for 2 weeks by oral gavage ($n = 10$ per group). Lungs were excised from sacrificed mice and lung metastases were scored. Experiments were conducted following an IACUC-approved protocol.

TUNEL assays

The in situ TUNEL assay was performed using the TUNEL Detection Kit (VitroVivo Biotech). Paraffin-embedded sections were mounted, dewaxed with xylene, and rehydrated. Labeled nick ends of DNA strands were visualized with 3,3′-diaminobenzidine (DAB). Counterstaining was with hematoxylin. DNase-treated sections were positive controls.

Immunohistochemistry

The streptavidin–biotin method was used for Immunohistochemistry (IHC) detection. Antigen retrieval was by heat treatment with citrate buffer. Endogenous peroxidase activity was blocked using 2% hydrogen peroxide in PBS. Nonspecific protein blocking was with 1% BSA and normal donkey or goat serum. Incubation with primary antibody was overnight at 4°C and the secondary antibody and streptavidin-HRP incubations were at room temperature for 40 minutes each. Primary antibody was replaced with PBS for a negative control. Antigen–antibody complex was visualized with the DAB chromogen. Antibodies were: Ki-67 (ab15580; Abcam; 1:1,000), phospho-RB (Ser807/811; No. 8516; Cell Signaling Technology; 1:200), MCL1 (No. 39224; Cell Signaling Technology; 1:50), phospho-FAK (Tyr397; No. 700255, Thermo Fisher Scientific, 1:2,000), and phospho-Src (Tyr418; ab4816; Abcam; 1:40). IHC scoring was by a pathologist unaware of the prior treatment arms.

In vivo mitosis analysis

Lung cancer xenografts were fixed with 10% formalin immediately after resection and were paraffin-embedded. Specimens were probed with phospho-histone H3 (Ser10) antibody (9701, Cell Signaling Technology; 1:200) and counterstained with hematoxylin. Stained cells were scored for multipolar mitotic cells using an Eclipse TE 2000-E microscope (Nikon).

Statistical analysis

Differences between analyzed groups were assessed by a Student *t* or Mann–Whitney *U* test. To control the overall type I error rate in multiple comparisons, Tukey method was used for pairwise comparisons. Dunnett method was applied for comparing the result of different drug concentrations with controls. Tumor growth was analyzed using the mixed model analysis. Kaplan–Meier survivals were by the log-rank test. Statistical analyses were with SPSS Statistics software (version 23, SPSS) and GraphPad Prism software (version 8, GraphPad Software). All statistical tests were two-sided; a *P* value of <0.05 was considered statistically significant.

Results

CYC065 effects in lung cancer cells

Antiproliferative effects of CYC065 were independently examined using multiple murine (ED1, LKR13, 393P, 344SQ, and KC2) and human (H522, H1299, Hop62, and A549) lung cancer cell lines. CYC065 treatment decreased proliferation in a dose- and time-dependent manner (**Fig. 1A**). Substantial antiproliferative effects of CYC065 were less evident in C10 murine immortalized pulmonary epithelial cells and BEAS-2B human immortalized bronchial epithelial cells than in the examined lung cancer cells (**Fig. 1A**). At the CYC065 0.5 μmol/L or lower concentrations, growth-inhibitory effects were modest in immortalized pulmonary epithelial cells (C10 and BEAS-2B) whereas lung cancer cellular growth profiles were markedly inhibited (**Fig. 1A**). Proliferation assay results were confirmed and extended in a high-throughput screen of 84 human lung cancer cell lines (Supplementary Table S1). At the CYC065 0.5 μmol/L dosage (where growth of immortalized epithelial cells was not appreciably affected), more than half of lung cancer cells were inhibited in their growth to less than 50% of controls in this high-throughput assay (**Fig. 1B**). Notably, *KRAS* oncoprotein expressing lung cancer cells were responsive to CYC065 treatment. This was similar to that seen in KRAS WT lung cancer cells (**Fig. 1C**). Growth inhibition by CYC065 treatment of lung cancer cells was only partially reversed after drug washout, indicating irreversible mechanisms were engaged in these antiproliferative effects (**Fig. 1D**).

Apoptosis induction and cell-cycle arrest after CYC065 treatments were examined in lung cancer cells. CYC065 treatment augmented apoptosis in murine (ED1, LKR13, 393P, 344SQ, and KC2) and human (H522, H1299, Hop62, and A549) lung cancer cells without appreciable effects observed in immortalized lung epithelial cells (C10 and BEAS-2B cells; **Fig. 1E**). CYC065 treatment caused G_1 arrest in the examined lung cancer cells (**Fig. 1F**).

Anaphase catastrophe as a general antineoplastic mechanism

One antineoplastic mechanism engaged by CDK2 inhibitors is induced anaphase catastrophe (12–16). To investigate this further, multipolar anaphases after CYC065 treatment were scored in lung cancer cells by respective staining for γ-tubulin, α-tubulin, and DNA in **Fig. 2A**. CYC065 treatment caused multipolar anaphase catastrophe in murine and human lung cancer cells, but not appreciably in C10 or BEAS-2B immortalized epithelial cells (**Fig. 2B**). Anaphase catastrophe occurs via inhibition of supernumerary centrosomes clustering after treatment with CDK2 inhibitors (14, 16, 17). To determine CYC065 treatment effects on centrosome clustering, cell populations with centrosome clustering were determined. Clustering of supernumerary centrosome appear in **Fig. 2A**. CYC065 inhibited clustering of supernumerary centrosomes (**Fig. 2C**).

To assess whether anaphase catastrophe occurred in other cancers, colon and pancreatic cancer cells were treated with CYC065. CYC065 treatment substantially inhibited proliferation (**Fig. 2D**) and induced apoptosis (**Fig. 2E**) in colon (DLD1 and HCT116) and pancreatic (PSN1 and AsPC1) cancer cells. The less evident effects in AsPC1 cells versus other examined cancer cells on days 2 and 3 were more prominent on day 4 of treatment. This was likely due to AsPC1 cells having much longer doubling times than the other studied cell lines (Supplementary Figs. S1B and S1C). Multipolar anaphase occurred after CYC065 treatment of colon (DLD1 and HCT116) and pancreatic (PSN1 and AsPC1) cancer cells (**Fig. 2F**). CYC065 treatment had analogous effects in lymphoma cells (Supplementary Fig. S2), indicating anaphase catastrophe induction by CDK2 inhibition is a broadly active mechanism.

Mechanisms of CYC065 actions

To determine how CDK2 and CDK9 contribute to the antineoplastic effects of CYC065, CDK2 and CDK9 were transfected individually into lung cancer cells (**Fig. 3A**). Gain of expression of CDK2 or CDK9 partially antagonized growth-inhibitory effects and apoptosis-induction after CYC065 treatment (**Fig. 3B** and **C**), indicating that CDK2 and CDK9 contribute to CYC065 antineoplastic effects. Yet, anaphase catastrophe-induction by CYC065 treatment was antagonized only after gain of CDK2 expression (**Fig. 3D**). Anaphase catastrophe was preferentially conferred by CDK2 inhibition following CYC065 treatment. This is consistent with work reporting that anaphase catastrophe was engaged by inhibition of CDK1 or CDK2, but not by CDK5 or CDK9 (15).

Protein expression profiles after CYC065 treatment

To elucidate mechanisms that engage antineoplastic effects of CYC065 in addition to induced-anaphase catastrophe, protein expression profiles were comprehensively explored following CYC065 treatment using Reverse phase protein arrays (RPPAs). Expression profiles of more than 300 growth regulatory proteins were independently interrogated after 6, 12, 24, and 48 hours of CYC065 relative to vehicle treatments of murine (344SQ and KC2) and human (H1299 and A549) lung cancer cells. When proteins were clustered according to the expression changes after CYC065 treatment, specific species were highlighted as statistically significantly upregulated or downregulated (or unchanged) across the studied lung cancer cells and time points. Upregulated proteins included those involved in DNA damage or apoptosis induction. Along with known CDK2 or CDK9 targets like RB protein phosphorylation (Ser807/811) and MCL1, proteins that were downregulated included FAK phosphorylation (Tyr397) and Src phosphorylation (Tyr416) that regulate metastasis (Supplementary Fig. S3; refs. 44, 45). Downregulation of these proteins by CYC065 treatment was confirmed by IHC (**Fig. 6**). Individually engineered gain of MCL-1 expression in HOP62 and H1299 lung cancer cells had minimal effects on induced apoptosis or growth inhibition following CYC065 treatment (Supplementary Fig. S4).

CYC065 treatment and lung cancer cell migration, invasion, and proliferation

On the basis of the RPPA results, it was hypothesized that CYC065 treatment inhibited metastatic properties of lung cancer cells. CYC065 effects on cell migration and invasion were explored using the metastasis-prone murine (344SQ and KC2; ref. 36) and human (H1299 and A549) lung cancer cells. Scratch and transwell migration assays, respectively, revealed that CYC065 treatment inhibited migration of these lung cancer cells (**Fig. 4A** and **B**). Matrigel invasion chamber assays showed that invasive properties of these lung cancer cells were
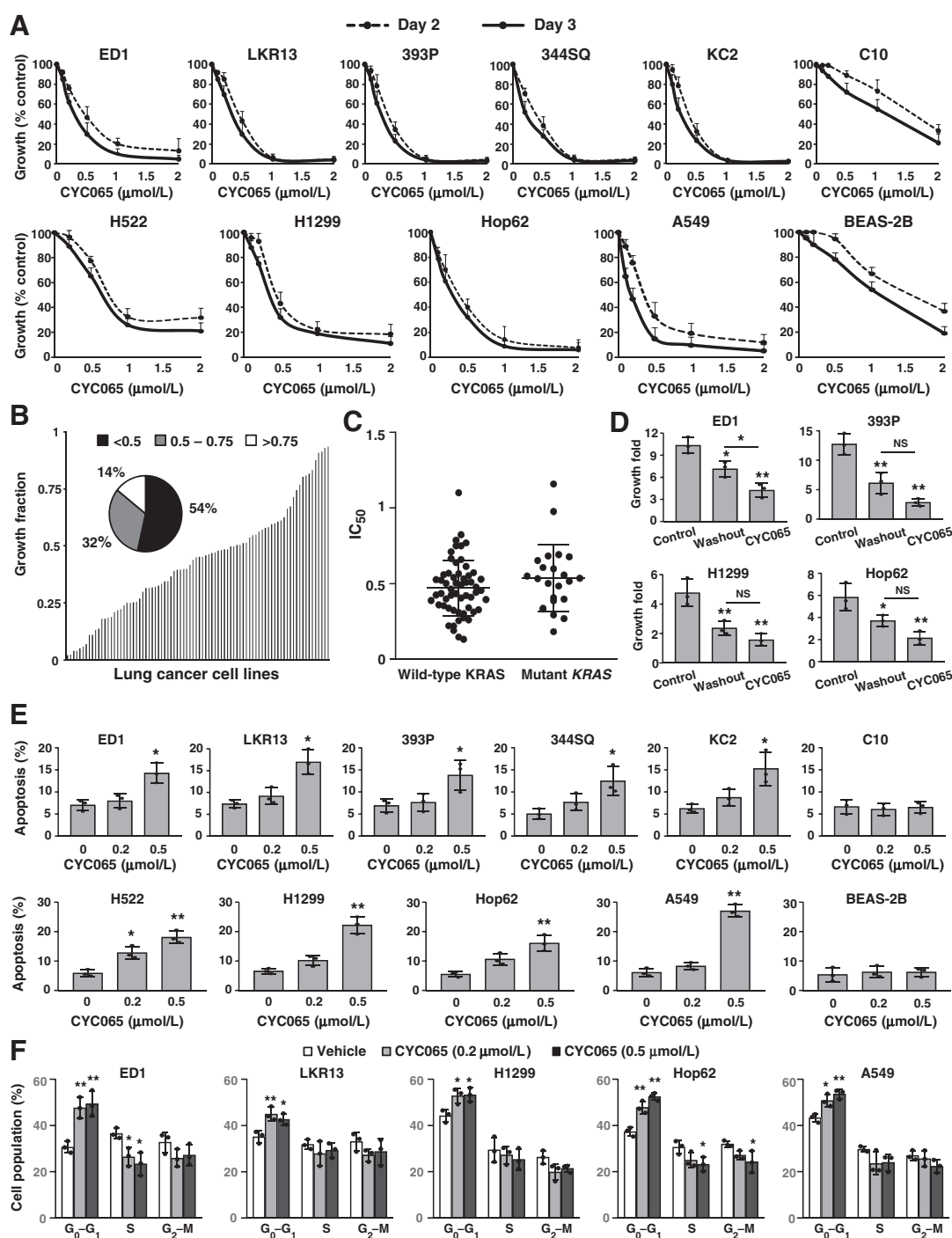
Figure 1.
Antineoplastic effects of CYC065 treatment in murine and human lung cancer cells. **A,** Dose-response consequences of CYC065 treatment in murine (ED1, LKR13, 393P, 344SQ, and KC2) and human (H522, H1299, Hop62, and A549) lung cancer cells. Effects on murine immortalized pulmonary epithelial cells (C10) and human immortalized bronchial epithelial cells (BEAS-2B) are shown. **B,** Relative proliferation is shown for 84 lung cancer cells in a high-throughput screen after CYC065 0.5 μmol/L treatment versus vehicle controls. Each bar displays an individual lung cancer cell line. The pie chart shows that the cell population was stratified by relative viability after CYC065 0.5 μmol/L treatment (vs. vehicle controls) among 84 lung cancer cell lines. **C,** Comparison of growth inhibitory effects of CYC065 treatment in KRAS wild-type versus mutant lung cancer cells were displayed using a high-throughput screen of 84 human lung cancer cells. Each symbol displays an individual cell line. **D,** Comparisons of CYC065 effects on growth of lung cancer cells versus vehicle controls, washout (CYC065 washout after 24 hours treatment), and CYC065 continuously-treated groups. Fold-growth versus day 0 are shown. **E,** Percentages of apoptotic cells are displayed after individual CYC065 treatment in murine and human lung cancer cells. Effects in C10 and BEAS-2B cells are displayed. **F,** Cell-cycle analysis after CYC065 treatment appear for murine and human lung cancer cells. Error bars are standard deviations with *, $P < 0.05$ and **, $P < 0.01$ by Tukey's multiple comparison test (**D**) and Dunnett multiple comparison t test (vs. controls; **E** and **F**).
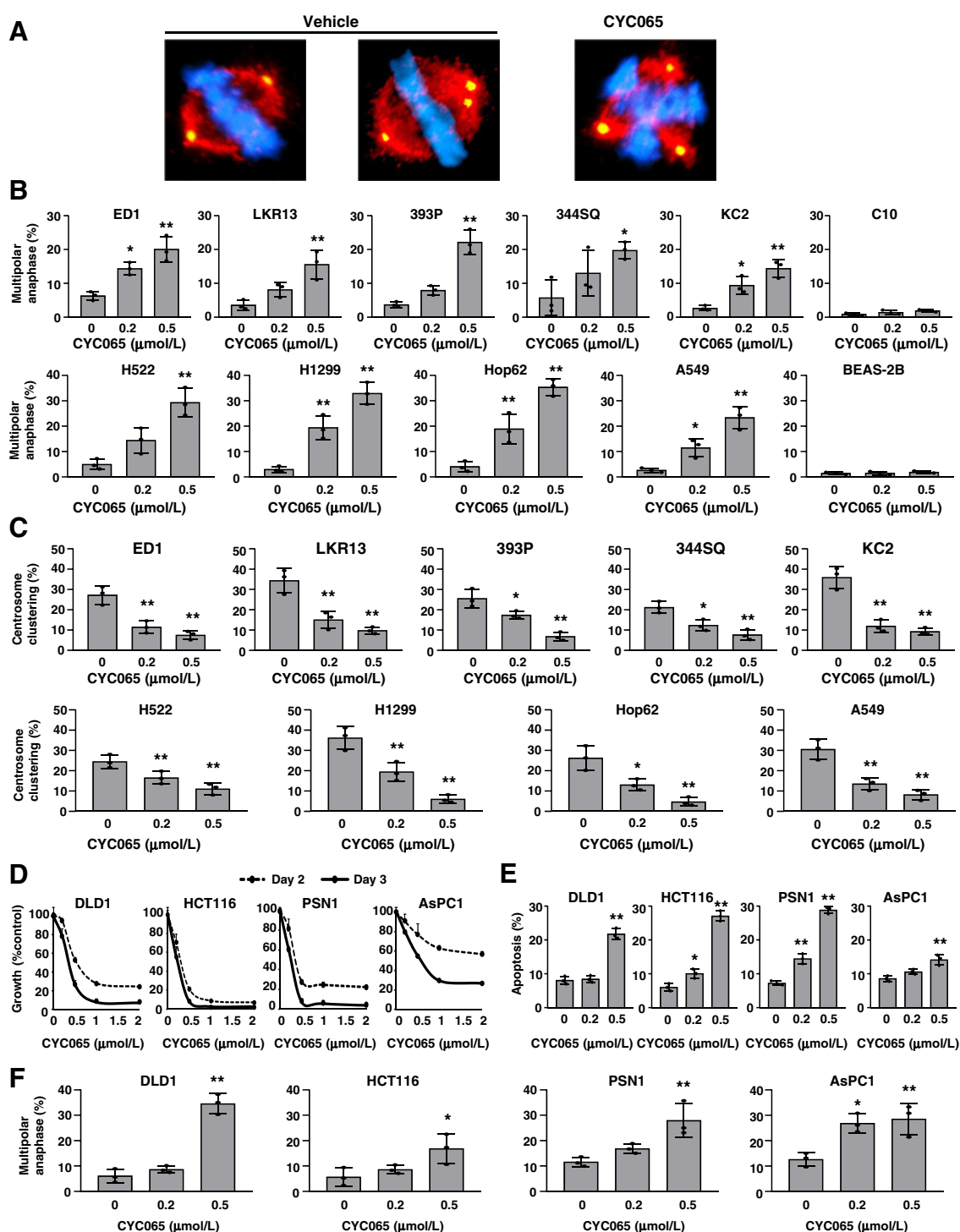
Figure 2.
Anaphase catastrophe is a broadly active antineoplastic mechanism. **A,** Representative immunofluorescent images of spindles from bipolar cells with two centrosomes (left), cells with clustered supernumerary centrosomes (middle), and cells with supernumerary centrosomes (right). The blue signal is Hoechst staining of DNA, red signal is α-tubulin staining, and green signal is γ-tubulin staining. **B,** Percentages of cells undergoing multipolar anaphase among anaphase cells after CYC065 treatment are displayed for murine (ED1, LKR13, 393P, 344SQ, and KC2) and human (H522, H1299, Hop62, and A549) lung cancer cells as well as for immortalized (C10 and BEAS-2B) lung epithelial cells. **C,** Percentages of cells with centrosome clustering among anaphase cells after CYC065 treatment are shown. **D,** Dose-responsive consequences of CYC065 treatment in colon (DLD1 and HCT116) and pancreatic (PSN1 and AsPC1) cancer cells. **E,** Percentages of apoptotic cells after CYC065 treatment are displayed in colon and pancreatic cancer cells. **F,** Percentages of cells undergoing multipolar anaphase after CYC065 treatment are shown in colon and pancreatic cancer cells. Error bars are SDs with *, $P < 0.05$ and **, $P < 0.01$ by Dunnett multiple comparison t test (vs. controls).
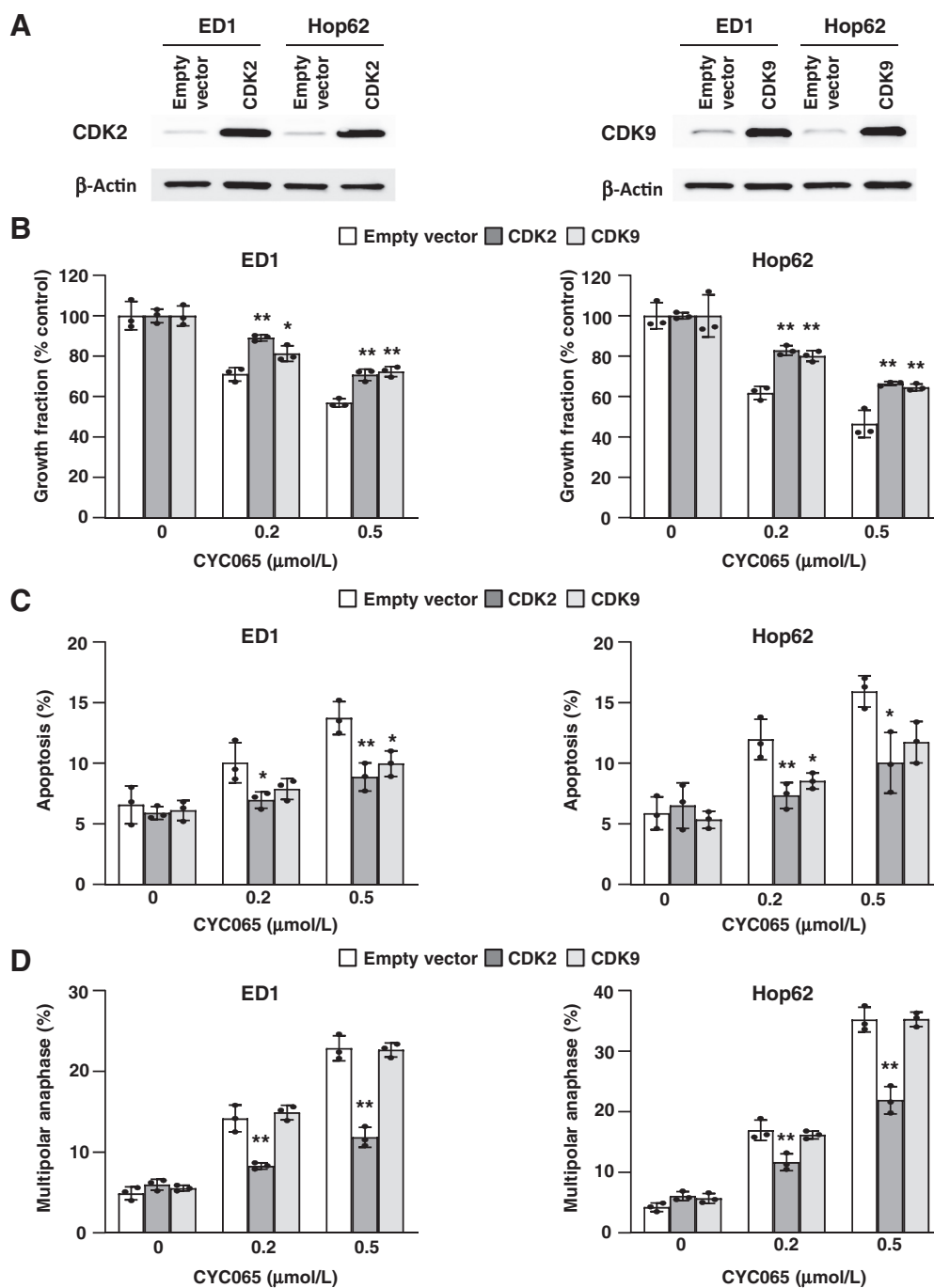
Figure 3.
Consequences of engineered gain of CDK2 or CDK9 expression on CYC065 treatment effects are shown in lung cancer cells. **A,** Immunoblot analyses after transfection of CDK2 or CDK9 expressing plasmids. **B,** CYC065 treatment effects are shown for lung cancer cell proliferation after engineered gain of CDK2 or CDK9 expression. **C,** Effects of CYC065 treatment on apoptosis induction after engineered gain of CDK2 or CDK9 expression in lung cancer cells are presented. **D,** Effects of CYC065 treatment on anaphase catastrophe after independent gain of CDK2 or CDK9 expression in lung cancer cells are displayed. Error bars are SDs with *, $P < 0.05$ and **, $P < 0.01$ by the Dunnett multiple comparison t test (vs. controls).

reduced by CYC065 treatment (**Fig. 4C**). Independently engineered gain of FAK or Src expression in A549 and H1299 lung cancer cells partially rescued the consequences of CYC065 treatment on migration and invasion with effects of gain of FAK expression more evident than for Src (Supplementary Fig. S5).

In vivo tumorigenicity after CYC065 treatment

CYC065 antitumorigenicity effects were studied in murine lung cancer models. The _KRAS_ oncoprotein-driven 393P and ED1SQ4 KRAS WT murine lung cancer cell lines were each engineered to express luciferase. Cells were subcutaneously injected into
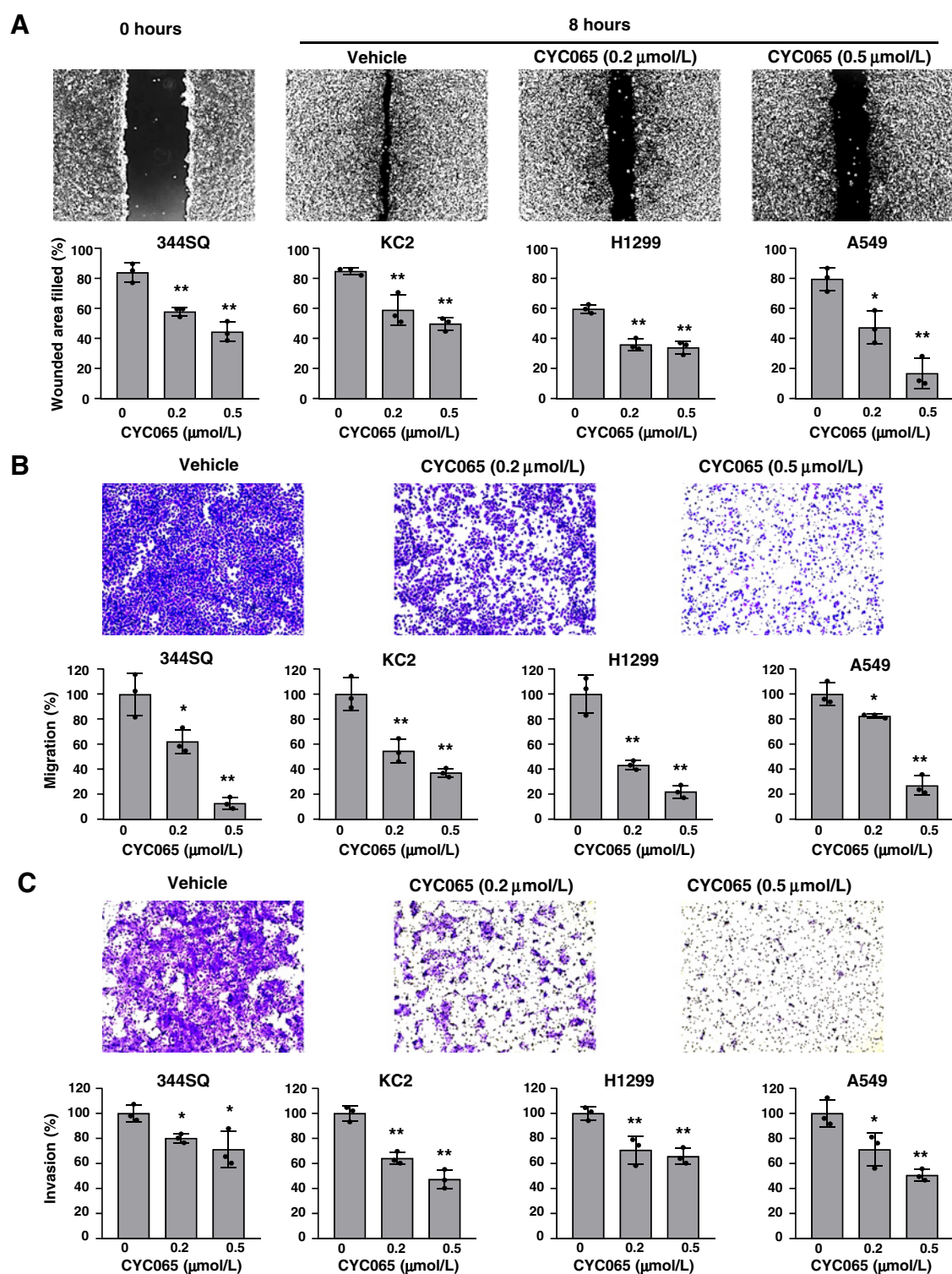
Figure 4.
CYC065 effects on lung cancer cell migration and invasion. **A,** Percentages of wounded area filled by migrating cells after 6 to 12 hours of independent vehicle or CYC065 treatment of murine (344SQ and KC2) and human (H1299 and A549) lung cancer cells are displayed. Representative images of wounded areas before and after treatment with vehicle or CYC065 treatments are provided. **B,** Percentages of migrated cells after independent vehicle or CYC065 treatment of murine and human lung cancer cells are presented. Representative images of migrating cells after vehicle or CYC065 treatment are shown. **C,** Percentages of lung cancer cell invasion after independent vehicle or CYC065 treatment are displayed. Representative images of invading cells after vehicle or CYC065 treatment are shown. Error bars display SDs with *, $P < 0.05$ and **, $P < 0.01$ by Dunnett multiple comparison t test (vs. controls).

immunocompetent syngeneic mice. Mice were treated with vehicle or CYC065. In 393P and ED1SQ4 syngeneic murine lung cancer models, tumor growth was repressed, and the excised tumor weights after these treatments were significantly ($P < 0.01$) reduced in CYC065-treated versus vehicle controls (**Fig. 5A** and **B**). Tumor burdens were evaluated by bioluminescent imaging. There was a statistically significant lower increase in bioluminescence in CYC065-treated mice than syngeneic lung cancer controls (**Fig. 5C**). These mice were treated with well-tolerated CYC065 dosages (55 mg/kg for 129S2/SVPasCrl and 75 mg/kg for FVB/N mice). To examine even higher CYC065 dosages, antitumorigenic effects were studied at 90 mg/kg for murine 393P and at 110 mg/kg dosages for ED1SQ4 murine cancer cells after subcutaneous injection into syngeneic mice. Enhanced antitumorigenic effects occurred at these CYC065 treatment dosages (Supplementary Fig. S6A), but with toxicity (weight loss).

These findings indicate a need for examining CYC065 in a combination regimen. Pretreatment with taxol augmented CYC065 treatment effects in Supplementary Fig. S6B. To elucidate mechanisms responsible for CYC065 antineoplastic effects, kinetic studies were done in A549 human lung cancer cells. Studies revealed minimal changes in senescence, but prominent induction of growth inhibition, G_1 arrest, apoptosis, and anaphase multipolarity. G_1-arrested cell progression was not fully blocked by treatment with the reversible CDK2/9 inhibitor CYC065; induced anaphase multipolarity was evident (Supplementary Figs. S6C and S7). Nocadozole-induced growth arrest did not prevent CYC065 response (Supplementary Fig. S7).

To assess the antineoplastic effects of CYC065 treatment, multiple lung cancer PDX models were examined (Supplementary Table S2). CYC065 treatment inhibited lung cancer xenograft growth in these PDX models, independent of *KRAS* oncoprotein expression (**Fig. 5D**). Final tumor weights after treatment were significantly reduced ($P < 0.05$) in CYC065-treated versus vehicle-treated mouse models (**Fig. 5E**).

In vivo effects of CYC065 treatment on lung cancer metastasis were analyzed using a syngeneic tail–vein injection lung cancer model. Metastasis-prone 344SQ cells were injected into the indicated mice; lung tumors were scored. Representative images of excised lungs harboring lung cancers appear in **Fig. 5F**. CYC065 treatment significantly ($P < 0.01$) reduced metastasis of 344SQ lung cancer cells (**Fig. 5F**). Histopathologic analysis of hematoxylin-eosin–stained sections of resected lung tissues were performed. Representative images in **Fig. 5G** reveal the decreased number and size of metastasized tumors after CYC065 treatment.

Changes in CYC065-treated lung cancer PDXs

In vivo expression profiles of candidate CYC065-regulated markers of response were analyzed immunohistochemically in lung cancer PDX models (TC464 and TC494). CYC065 treatment reduced staining of the proliferative marker Ki-67 and increased apoptosis scored by TUNEL assays in these PDX models (**Fig. 6A**).

Expression levels of RB phosphorylation (Ser807/811) (a CDK2 target), MCL1(a CDK9 target), FAK phosphorylation (Tyr397), and Src phosphorylation (Tyr416), which were highlighted by RPPAs as downregulated after CYC065 treatment, were each investigated by IHC assays in these PDX models (TC464 and TC494). Representative immunostained images appear in **Fig. 6B**. CYC065-regulated proteins were repressed by CYC065 treatment (**Fig. 6B**).

To examine *in vivo* CYC065 treatment effects on mitosis, lung cancer xenografts were stained with phospho-histone H3 after vehicle or CYC065 treatment in **Fig. 6C**. Percentages of aberrant mitoses with

multipolar segregation of chromosomes (indicating presence of anaphase catastrophe) increased in CYC065-treated lung tumors versus vehicle controls (**Fig. 6C**). Thus, *in vitro* CYC065 treatment effects were confirmed in the *in vivo* setting.

Discussion

The clinical-lead CDK2/9 inhibitor CYC065 exerts antineoplastic effects against diverse aneuploid cancers, including lung cancer. One notable mechanism engaged by CYC065 treatment was anaphase catastrophe after CDK1 or CDK2 antagonism (12–17). This study advances prior work by showing that anaphase catastrophe occurred *in vivo* in lung cancer PDX models following CYC065 treatment. Prior work using siRNAs targeting individual CDKs revealed that anaphase catastrophe was enhanced by inhibition of CDK1 or CDK2, but not by CDK5 or CDK9 (15). Consistent with this, anaphase catastrophe induction by CYC065 treatment was antagonized by engineered gain of CDK2 but not by CDK9 expression (**Fig. 3**).

Because anaphase catastrophe occurs preferentially in cells with supernumerary centrosomes, engaging this pathway is a way to combat cancers with supernumerary centrosomes (13, 14, 46). CYC065 treatment effects were minimal in immortalized murine pulmonary and human bronchial epithelial cells. CDK2 inhibitors augmented anaphase catastrophe in lung cancer cells (12, 15, 16). That work was extended here by confirming that anaphase catastrophe increased after CYC065 treatment of lung and other aneuploid cancers including lymphoma, colon, and pancreatic cancers. Anaphase catastrophe is a broadly active induced pharmacologic mechanism.

Induced anaphase catastrophe engages multipolar chromosome mis-segregation. Hence, combination CYC065 treatments with other chromosome segregation regulators are appealing. The microtubule-targeting agent taxol promotes improper chromosome alignment and chromosome mis-segregation (47). CDK2 inhibitors (seliciclib and dinaciclib) conferred synergistic or additive antineoplastic effects against lung cancer when combined with a taxane (12, 15). Pretreatment with taxol increased CYC065 antineoplastic effects in lung cancer cells (Supplementary Fig. S6B). Cooperative antineoplastic effects occurred with PLK4 inhibition (48). Consistent with this, the CDK2 inhibitor seliciclib augmented antineoplastic effects of a PLK4 inhibitor that promotes centriole duplication (49). Similar cooperation might occur with CYC065 treatment and should be explored.

RPPA profiles performed in lung cancer cells after CYC065 treatment versus controls highlighted species that could mediate antineoplastic effects of CYC065 beyond induced-anaphase catastrophe. These include the known CDK2 inhibition target, RB phosphorylation, and the CDK9 inhibition target, MCL1. Inhibition of RB phosphorylation and MCL1 protein expression might individually or cooperatively affect CYC065 antineoplastic activity.

FAK phosphorylation and Src phosphorylation profiles were repressed. These species regulate metastasis (44, 45). This prompted studies of the antimetastatic effects of CYC065. CYC065 treatment inhibited lung cancer metastasis, a major cause of lung cancer mortality (50, 51). Future work should learn if CDK2 directly affects FAK or Src proteins. Notably, individually engineered gain of FAK or Src expression partially reversed CYC065 inhibitory effects on migration and invasion in lung cancer cells (Supplementary Fig. S4). Future work will determine if CDK2 inhibition represses lung cancer metastases in other models.

Antineoplastic effects of CYC065 were extended using multiple lung cancer PDX models. These informative models could predict clinical

Kawakami et al.
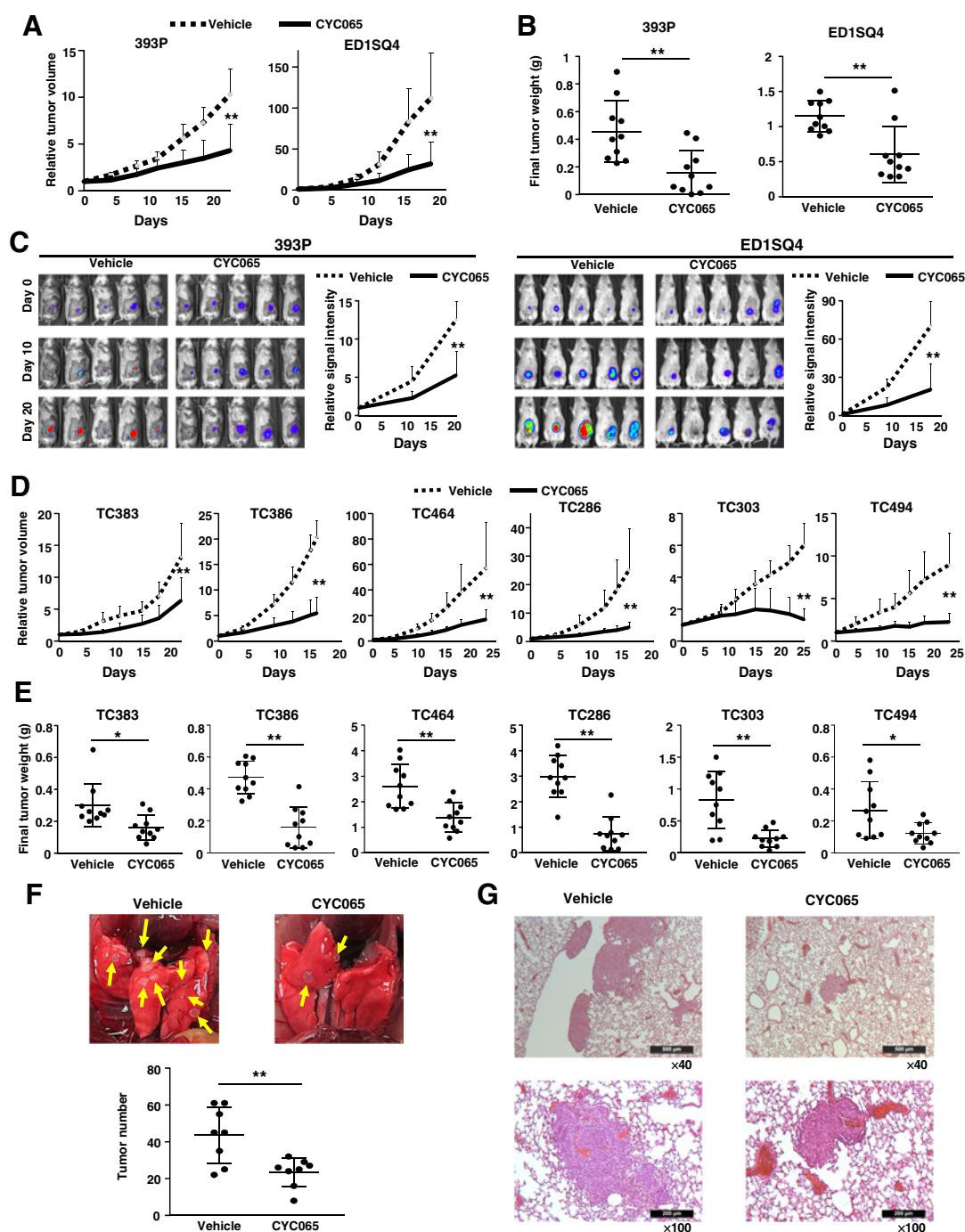
Figure 5.
In vivo CYC065 antitumorigenic effects. **A,** Comparison of tumor growth in syngeneic murine lung cancer xenograft models treated with vehicle or CYC065. Day 0 is the treatment start date. Error bars are standard deviations with **, $P < 0.01$ by the mixed model analysis. **B,** Comparisons of tumor weights in syngeneic murine lung cancer models aftertreatments. Each symbol represents a single mouse. Bars represent mean values and SDs with **, $P < 0.01$ by the Student t test. **C,** Bioluminescent signals are shown from tumors arising from syngeneic murine lung cancer models treated with vehicle or CYC065. Representative bioluminescence images from these mice appear over time. Error bars represent standard deviations with **, $P < 0.01$ by the mixed model analysis. **D,** Comparisons are shown for tumor growth in lung cancer PDX models treated with vehicle or CYC065. Day 0 is the treatment start date. Error bars represent SDs with **, $P < 0.01$ by the Student t test. **E,** Comparisons of tumor weights are presented for lung cancer PDX models after treatments with vehicle or CYC065. Each symbol represents a single mouse. Bars represent mean values and SDs with *, $P < 0.05$ and **, $P < 0.01$ by the Student t test. **F,** Lung tumor formation is provided for a syngeneic tail–vein injection model using metastasis-prone 344SQ cells after treatments with vehicle or CYC065. Representative images of lung tissues are shown. Yellow arrows highlight metastatic tumors. Bars represent mean values and SDs with **, $P < 0.01$ by the Student t test. **G,** Representative hematoxylin-eosin–stained photomicrographs of resected lung tissues after treatments with vehicle or CYC065 are provided.
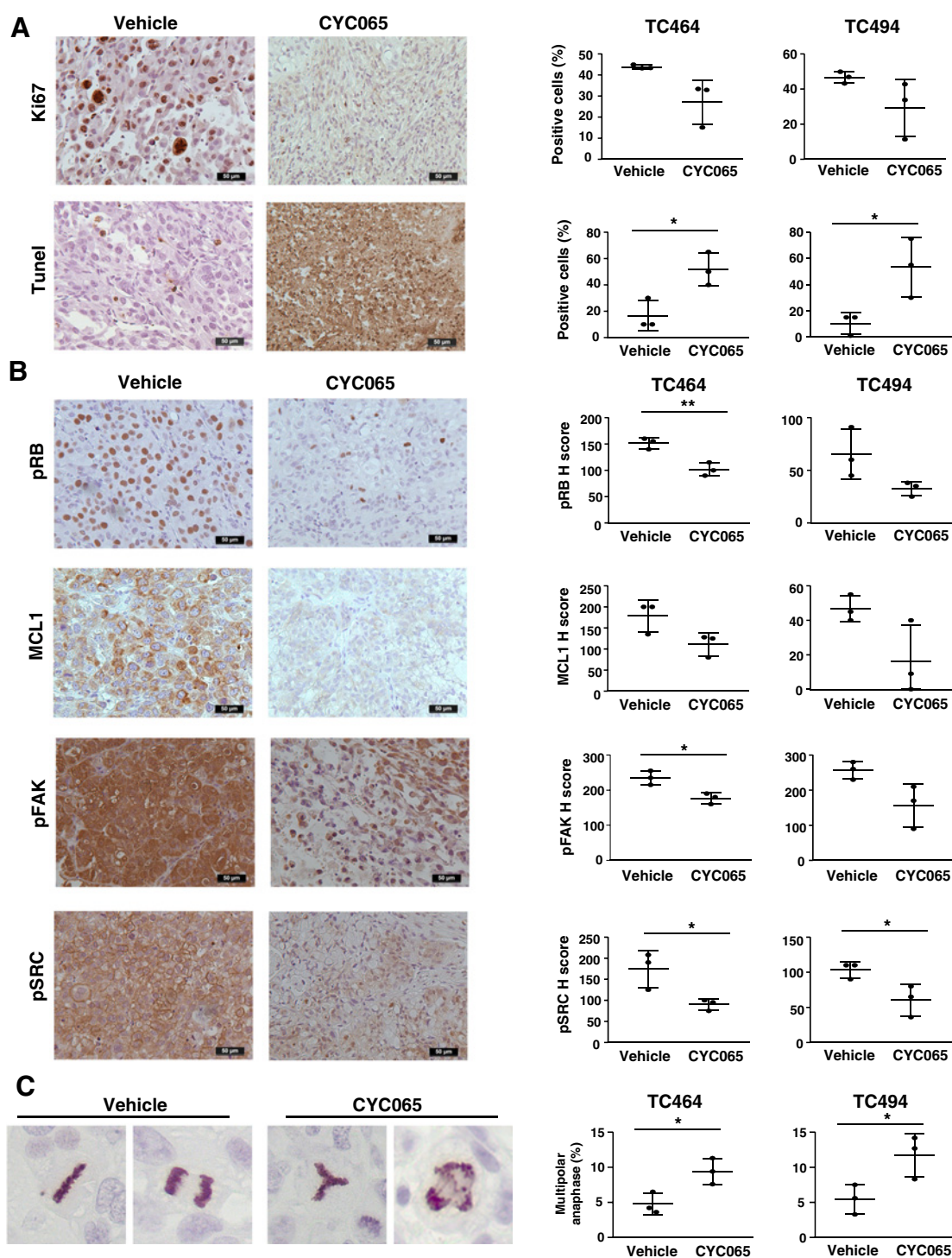
Figure 6.
In vivo protein expression profiles after CYC065 treatment. **A,** Comparisons appear for Ki-67 staining and TUNEL assay for scoring of apoptotic cells in lung cancer PDX models after independent treatments with vehicle or CYC065. Each symbol is a single mouse. Representative immunostained images comparing vehicle and CYC065-treated groups are displayed (left). Bars represent mean values and SDs with *, $P < 0.05$ by the Student t test. **B,** Comparisons of profiles in lung cancer PDX models after treatments with vehicle or CYC065. Each symbol is a single mouse. Representative immunostained images of each species from vehicle or CYC065-treated groups are shown. Bars represent mean values and SDs with *, $P < 0.05$ and **, $P < 0.01$ by the Student t test. **C,** Analysis of mitosis is shown by phospho-histone H3 Ser10 immunostaining of lung cancer PDX models after treatments with vehicle or CYC065. Representative phospho-histone H3 Ser10 immunostained images that indicate bipolar mitosis in the vehicle-treated group and multipolar mitosis in the CYC065-treated group are displayed. Percentages of cells with multipolar mitosis in lung cancer PDX models after vehicle or CYC065 treatments are shown. Bars represent mean values and SDs *, $P < 0.05$ by the Student t test.

activities of CYC065. CYC065 treatment elicited antitumor effects in these PDX models, despite *KRAS* oncoprotein expression. Treatment of lung cancers that harbor *KRAS* oncoprotein expression is an unmet medical need (20). CYC065 is a CDK2/9 inhibitor in two phase I clinical trials (29, 30). In one trial, durable stable disease followed CYC065 administration (29). Lung cancer cases were not appreciably accrued to this trial and should be in future ones.

CYC065 exerted antineoplastic effects on lung cancers in diverse preclinical models, including PDX models. These studies provide a rationale for treating human lung cancer cases with CYC065. TCGA data revealed that expression profiles of CDK2 or its partner cyclin E are statistically significantly higher in diverse cancers including lung cancers versus adjacent histopathologically normal lung. This was associated with an unfavorable clinical survival (Supplementary Figs. S8 and S9), indicating the clinical relevance of CDK2 and cyclin E profiles in human lung and perhaps other cancers to guide clinical use of CYC065. Engagement of CDK2-dependent phosphorylation of RB can mediate resistance to inhibition of CDK4 and CDK6 in a lung cancer mouse model, implying that CDK2 antagonism is a lung cancer therapeutic target (52, 53). These findings provide a rationale for use of CYC065 treatment for lung and other cancers, perhaps when combined with agents like taxol (Supplementary Fig. S6B).

Syngeneic and PDX tumor growth assays showed CYC065 reduced tumor growth (**Fig. 5**). Higher CYC065 treatment dosages exerted greater antitumorigenic effects (Supplementary Fig. S6A). Differences in CYC065 toxicity profiles exist between mouse models and clinical trials in patients. Kinetic studies in human lung cancer cells indicate that induced anaphase catastrophe is prominent after CYC065 treatment. Interestingly when G_1 arrest occurred, it did not confer CYC065 resistance (Supplementary Fig. S7).

IHC analysis of lung cancer PDXs following CYC065 treatment confirmed the downregulation of key growth regulatory proteins (RB phosphorylation, MCL1, FAK phosphorylation, and Src phosphorylation), as predicted by the RPPA findings (Supplementary Fig. S3). These species are potential clinical markers of CYC065 response. CYC065 treatment effects are likely due to cooperative mechanisms in concert with engaged anaphase catastrophe. Antineoplastic effects of CYC065 were antagonized by the engineered gain of CDK2 or CDK9 expression, indicating that CDK2 and CDK9 contribute to aspects of CYC065 treatment effects. Yet, only CDK2-antagonism caused anaphase catastrophe. Future work should precisely determine the single cell fates after CYC065 treatment.

The next-generation CDK2/9 inhibitor CYC065 confers antineoplastic effects including antimetastatic activities that collectively were independent of *KRAS* oncoprotein expression in the studied tumors. Findings presented here reveal that CDK2 antagonism mediates the induction of anaphase catastrophe. This is a broadly active mechanism that can be engaged to eradicate aneuploid cancers even when *KRAS* mutations are present. These findings should guide the design of future clinical trials using this novel CDK2/9 antagonist.

Authors' Contributions

M. Kawakami: Conceptualization, resources, data curation, formal analysis, validation, investigation, visualization, methodology, writing–original draft. **L.M. Mustachio:** Resources, data curation, investigation, methodology. **Y. Chen:** Resources, data curation, investigation. **Z. Chen:** Resources, data curation, validation, investigation, methodology. **X. Liu:** Resources, data curation, validation, investigation, methodology. **C.-H. Wei:** Resources, data curation, formal analysis, validation, investigation, methodology. **J. Roszik:** Resources, data curation, software, formal analysis. **A.S. Kittai:** resources, data curation, investigation. **A.V. Danilov:** Resources, data curation, investigation. **X. Zhang:** Resources, data curation, investigation. **B. Fang:** Resources, data curation, investigation. **J. Wang:** Resources, data curation, software, formal analysis. **J.V. Heymach:** Resources, data curation. **L. Tyutyunyk-Massey:** Conceptualization, data curation, methodology, writing–review and editing. **S.J. Freemantle:** Conceptualization, resources, investigation, writing–review and editing. **J.M. Kurie:** Conceptualization, resources, formal analysis, supervision, investigation, project administration, writing–review and editing. **X. Liu:** Conceptualization, resources, formal analysis, supervision, investigation, project administration, writing–review and editing. **E. Dmitrovsky:** Conceptualization, resources, data curation, supervision, funding acquisition, investigation, methodology, project administration, writing–review and editing.

References

1. Hanahan D, Weinberg RA. Hallmarks of cancer: the next generation. Cell 2011; 144:646–74.
2. Lingle WL, Lutz WH, Ingle JN, Maihle NJ, Salisbury JL. Centrosome hypertrophy in human breast tumors: implications for genomic stability and cell polarity. Proc Natl Acad Sci U S A 1998;95: 2950–55.
3. Nigg EA. Centrosome aberrations: cause or consequence of cancer progression? Nat Rev Cancer 2002;2:815–25.
4. Kramer A, Neben K, Ho AD. Centrosome replication, genomic instability and cancer. Leukemia 2002;16:767–75.
5. Zyss D, Gergely F. Centrosome function in cancer: guilty or innocent? Trends Cell Biol 2009;19:334–46.
6. Chan JY. A clinical overview of centrosome amplification in human cancers. Int J Biol Sci 2011;7:1122–44.
7. Ring D, Hubble R, Kirschner M. Mitosis in a cell with multiple centrioles. J Cell Biol 1982;94:549–56.

8. Brinkley BR. Managing the centrosome numbers game: from chaos to stability in cancer cell division. Trends Cell Biol 2001;11:18–21.

9. Quintyne NJ, Reing JE, Hoffelder DR, Gollin SM, Saunders WS. Spindle multipolarity is prevented by centrosomal clustering. Science 2005;307: 127–29.

10. Kwon M, Godinho SA, Chandhok NS, Ganem NJ, Azioune A, Thery M, et al. Mechanisms to suppress multipolar divisions in cancer cells with extra centrosomes. Genes Dev 2008;22:2189–203.

11. Godinho SA, Kwon M, Pellman D. Centrosomes and cancer: how cancer cells divide with too many centrosomes. Cancer Metastasis Rev 2009;28:85–98.

12. Galimberti F, Thompson SL, Liu X, Li H, Memoli V, Green SR, et al. Targeting the cyclin E-Cdk-2 complex represses lung cancer growth by triggering anaphase catastrophe. Clin Cancer Res 2010;16:109–20.

13. Galimberti F, Thompson SL, Ravi S, Compton DA, Dmitrovsky E. Anaphase catastrophe is a target for cancer therapy. Clin Cancer Res 2011;17:1218–22.

14. Kawakami M, Mustachio LM, Liu X, Dmitrovsky E. Engaging anaphase catastrophe mechanisms to eradicate sneuploid cancers. Mol Cancer Ther 2018;17: 724–31.

15. Danilov AV, Hu S, Orr B, Godek K, Mustachio LM, Sekula D, et al. Dinaciclib induces anaphase catastrophe in lung cancer cells via inhibition of cyclin-dependent kinases 1 and 2. Mol Cancer Ther 2016;15:2758–66.

16. Kawakami M, Mustachio LM, Rodriguez-Canales J, Mino B, Roszik J, Tong P, et al. Next-generation CDK2/9 inhibitors and anaphase catastrophe in lung cancer. J Natl Cancer Inst 2017;109:djw297.

17. Hu S, Danilov AV, Godek K, Orr B, Tafe LJ, Rodriguez-Canales J, et al. CDK2 inhibition causes anaphase catastrophe in lung cancer through the centrosomal protein CP110. Cancer Res 2015;75:2029–38.

18. Hu S, Lu Y, Orr B, Godek K, Mustachio LM, Kawakami M, et al. Specific CP110 phosphorylation sites mediate anaphase catastrophe after CDK2 inhibition: evidence for cooperation with USP33 knockdown. Mol Cancer Ther 2015;14: 2576–85.

19. Aviel-Ronen S, Blackhall FH, Shepherd FA, Tsao MS. K-ras mutations in non-small-cell lung carcinoma: a review. Clin Lung Cancer 2006;8:30–8.

20. Roberts PJ, Stinchcombe TE. KRAS mutation: should we test for it, and does it matter? J Clin Oncol 2013;31:1112–21.

21. Finn RS, Martin M, Rugo HS, Jones S, Im SA, Gelmon K, et al. Palbociclib and letrozole in advanced breast cancer. N Engl J Med 2016;375:1925–36.

22. Hortobagyi GN, Stemmer SM, Burris HA, Yap YS, Sonke GS, Paluch-Shimon S, et al. Ribociclib as first-line therapy for HR-positive, advanced breast cancer. N Engl J Med 2016;375:1738–48.

23. Wilson SC, Atrash B, Barlow C, Eccles S, Fischer PM, Hayes A, et al. Design, synthesis and biological evaluation of 6-pyridylmethylaminopurines as CDK inhibitors. Bioorg Med Chem 2011;19:6949–65.

24. Frame S, Saladino C, MacKay C, Atrash B, Sheldrake P, McDonald E, et al. Fadraciclib (CYC065), a novel CDK inhibitor, targets key pro-survival and oncogenic pathways in cancer. PLoS One 2020;15:e0234103.

25. Scaltriti M, Eichhorn PJ, Cortes J, Prudkin L, Aura C, Jimenez J, et al. Cyclin E amplification/overexpression is a mechanism of trastuzumab resistance in HER2+ breast cancer patients. Proc Natl Acad Sci U S A 2011;108:3761–6.

26. Rao SS, Stoehr J, Dokic D, Wan L, Decker JT, Konopka K, et al. Synergistic effect of eribulin and CDK inhibition for the treatment of triple negative breast cancer. Oncotarget 2017;8:83925–39.

27. Thomas AL, Lind H, Hong A, Dokic D, Oppat K, Rosenthal E, et al. Inhibition of CDK-mediated Smad3 phosphorylation reduces the Pin1-Smad3 interaction and aggressiveness of triple negative breast cancer cells. Cell Cycle 2017;16:1453–64.

28. Cocco E, Lopez S, Black J, Bellone S, Bonazzoli E, Predolini F, et al. Dual CCNE1/PIK3CA targeting is synergistic in CCNE1-amplified/PIK3CA-mutated uterine serous carcinomas in vitro and in vivo. Br J Cancer 2016;115:303–11.

29. Do KT, Chau N, Wolanski A, Beardslee B, Hassinger F, Bhushan K, et al. Phase I safety, pharmacokinetic and pharmacodynamic study of CYC065, a cyclin dependent kinase inhibitor, in patients with advanced cancers (NCT02552953). In: Proceedings of the Annual Meeting of the American Association for Cancer Research 2018; 2018 Apr 14-18; Chicago, IL. Philadelphia (PA): AACR; Cancer Res 78:13s, 2018 (suppl; abstr CT037).

30. Chen R, Chen Y, Frame S, Blake D, Wierda WG, Zheleva D, et al. Strategic combination of the cuclin-dependent kinase inhibitor CYC065 with venotoclax to target anti-apoptotic proteins in chronic lymphocytic leukemia [abstract]. In: Proceedings of the Annual Meeting of the American Association for Cancer Research 2018; 2018 Apr 14-18; Chicago, IL. Philadelphia (PA): AACR; Cancer Res 78:13s, 2018 (suppl; abstr 3905).

31. Ma Y, Fiering S, Black C, Liu X, Yuan Z, Memoli VA, et al. Transgenic cyclin E triggers dysplasia and multiple pulmonary adenocarcinomas. Proc Natl Acad Sci U S A 2007;104:4089–94.

32. Freemantle SJ, Dmitrovsky E. Cyclin E transgenic mice: discovery tools for lung cancer biology, therapy, and prevention. Cancer Prev Res 2010;3:1513–8.

33. Liu X, Sempere LF, Ouyang H, Memoli VA, Andrew AS, Luo Y, et al. MicroRNA-31 functions as an oncogenic microRNA in mouse and human lung cancer cells by repressing specific tumor suppressors. J Clin Invest 2010;120:1298–309.

34. Wislez M, Fujimoto N, Izzo JG, Hanna AE, Cody DD, Langley RR, et al. High expression of ligands for chemokine receptor CXCR2 in alveolar epithelial neoplasia induced by oncogenic kras. Cancer Res 2006;66:4198–207.

35. Chen Y, Terajima M, Yang Y, Sun L, Ahn YH, Pankova D, et al. Lysyl hydroxylase 2 induces a collagen cross-link switch in tumor stroma. J Clin Invest 2015;125:1147–62.

36. Gibbons DL, Lin W, Creighton CJ, Rizvi ZH, Gregory PA, Goodall GJ, et al. Contextual extracellular cues promote tumor cell EMT and metastasis by regulating miR-200 family expression. Genes Dev 2009;23:2140–51.

37. Chen L, Diao L, Yang Y, Yi X, Rodriguez BL, Li Y, et al. CD38-mediated immunosuppression as a mechanism of tumor cell escape from PD-1/PD-L1 blockade. Cancer Discov 2018;8:1156–75.

38. Chou TC. Drug combination studies and their synergy quantification using the Chou-Talalay method. Cancer Res 2010;70:440–46.

39. Cheng KW, Lu Y, Mills GB. Assay of Rab25 function in ovarian and breast cancers. Methods Enzymol 2005;403:202–15.

40. Tibes R, Qiu Y, Lu Y, Hennessy B, Andreeff M, Mills GB, et al. Reverse phase protein array: validation of a novel proteomic technology and utility for analysis of primary leukemia specimens and hematopoietic stem cells. Mol Cancer Ther 2006;5:2512–21.

41. Iadevaia S, Lu Y, Morales FC, Mills GB, Ram PT. Identification of optimal drug combinations targeting cellular networks: integrating phospho-proteomics and computational network analysis. Cancer Res 2010;70:6704–14.

42. Hao C, Wang L, Peng S, Cao M, Li H, Hu J, et al. Gene mutations in primary tumors and corresponding patient-derived xenografts derived from non-small cell lung cancer. Cancer Lett 2015;357:179–85.

43. Pu X, Zhang R, Wang L, Chen Y, Xu Y, Pataer A, et al. Patient-derived tumor immune microenvironments in patient-derived xenografts of lung cancer. J Transl Med 2018;16:328.

44. Guan JL. Role of focal adhesion kinase in integrin signaling. Int J Biochem Cell Biol 1997;29:1085–96.

45. Steeg PS. Targeting metastasis. Nat Rev Cancer 2016;16:201–18.

46. Kawakami M, Liu X, Dmitrovsky E. New cell cycle inhibitors target aneuploidy in cancer therapy. Annu Rev Pharmacol Toxicol 2019;59:361–77.

47. Dominguez-Brauer C, Thu KL, Mason JM, Blaser H, Bray MR, Mak TW. Targeting mitosis in cancer: emerging strategies. Mol Cell 2015;60:524–36.

48. Holland AJ, Cleveland DW. Polo-like kinase 4 inhibition: a strategy for cancer therapy? Cancer Cell 2014;26:151–3.

49. Kawakami M, Mustachio LM, Zheng L, Chen Y, Rodriguez-Canales J, Mino B, et al. Polo-like kinase 4 inhibition produces polyploidy and apoptotic death of lung cancers. Proc Natl Acad Sci U S A 2018;115:1913–8.

50. Nguyen DX, Bos PD, Massague J. Metastasis: from dissemination to organ-specific colonization. Nat Rev Cancer 2009;9:274–84.

51. Chuang CH, Greenside PG, Rogers ZN, Brady JJ, Yang D, Ma RK, et al. Molecular definition of a metastatic lung cancer state reveals a targetable CD109-Janus kinase-Stat axis. Nat Med 2017;23:291–300.

52. Walter DM, Yates TJ, Ruiz-Torres M, Kim-Kiselak C, Gudiel AA, Deshpande C, et al. RB constrains lineage fidelity and multiple stages of tumour progression and metastasis. Nature 2019;569:423–7.

53. Rubin SM, Sage J. Manipulating the tumour-suppressor protein Rb in lung cancer reveals possible drug targets. Nature 2019;569:343–4.

AAGR American Association for Cancer Research

Molecular Cancer Therapeutics

A Novel CDK2/9 Inhibitor CYC065 Causes Anaphase Catastrophe and Represses Proliferation, Tumorigenesis, and Metastasis in Aneuploid Cancers

Masanori Kawakami, Lisa Maria Mustachio, Yulong Chen, et al.

Updated version	Access the most recent version of this article at: doi:10.1158/1535-7163.MCT-19-0987
Supplementary Material	Access the most recent supplemental material at: http://mct.aacrjournals.org/content/suppl/2020/12/04/1535-7163.MCT-19-0987.DC1

Cited articles	This article cites 51 articles, 21 of which you can access for free at: http://mct.aacrjournals.org/content/20/3/477.full#ref-list-1

E-mail alerts	Sign up to receive free email-alerts related to this article or journal.
Reprints and Subscriptions	To order reprints of this article or to subscribe to the journal, contact the AACR Publications Department at pubs@aacr.org.
Permissions	To request permission to re-use all or part of this article, use this link http://mct.aacrjournals.org/content/20/3/477. Click on "Request Permissions" which will take you to the Copyright Clearance Center's (CCC) Rightslink site.